

**A model-based approach to correcting spectral irradiance data  
using an upward-looking airborne sensor (CASI ILS)**  
Kyu-Young Choi and Edward J. Milton  
Department of Geography, University of Southampton,  
Highfield, Southampton SO17 1BJ  
renochoi@soton.ac.uk

## Abstract

A number of aircraft sensors have the facility to measure spectral downwelling irradiance using a sensor mounted on the roof of the aircraft, but these data are rarely used for atmospheric correction. Part of the problem is that the attitude of the airborne platform is always changing during flight, even in stable conditions, so that direct use of data from an incident light sensor (ILS) can introduce errors into atmospheric correction methods.

The continual motion of the ILS is used here to advantage, as a means to fit a sky radiance distribution model developed by [Brungar and Hooper \(1993\)](#) to data from the Itres Instruments CASI ILS. The inclination of the ILS sensor, due to changing aircraft attitude, is considered as the slope plane in the model. The selected model coefficients correspond to parameterised atmospheric conditions and represent atmospheric transmission and the proportion of direct:diffuse flux. The method was used to correct CASI ILS data acquired over a site in southern England. Comparison with spectral irradiance measured simultaneously on the ground shows that the method reduced the variability of the ILS data and also compensated for the effect of different flight directions. The sky radiance distribution at sensor level is also calculated by the model, and shows the characteristics of the sky conditions at the time of each flight.

## 1. Introduction

The calibration of remotely sensed data is becoming increasingly important, as the applications of the remote sensing (RS) require more accurate information. In addition to the basic radiometric calibration, atmospheric correction is often essential for multi-temporal RS applications, for those focusing on dark targets, or for those in which physically meaningful units (e.g. spectral radiance, reflectance or albedo) are required. Incomplete or inaccurate atmospheric correction often results in failure of the most common uses of image data, such as mapping land-cover and land-cover change ([Song \*et al.\*, 2001](#)).

Atmospheric correction of RS data from spaceborne sensors has been relatively well understood for many years, since it is simpler than that of airborne data. The relatively small field of view due to high altitude means less directional effects in reflected radiance from the ground, and more importantly, the radiance travels twice the complete thickness of the atmosphere between sensor and the ground target, and the solar irradiance at the top of the atmosphere is known. In airborne sensing, flying in the middle of the atmosphere, estimating atmospheric conditions is much more complicated than for spaceborne RS data. The altitude and direction of the flight are not always the same, resulting in changes in the sun-target-sensor geometry ([Wilson, 1995](#)). These result in variations in incident illumination and in the amount of atmospheric scattering above the sensor level ([Stokkum and Guzzi, 1984](#)).

The feasibility of using an airframe-mounted spectrometer to measure spectral irradiance at the sensor was investigated by [Milton \*et al.\* \(1994\)](#) using a Spectron Engineering SE-590 spectroradiometer. Two identical instruments, one with a cosine-corrected receptor for downwelling irradiance and the other with a nominal 1° field-of-view for upwelling radiance, were mounted outside the cabin of a Bell Jet Ranger helicopter. Multi-height measurements over uniform targets showed residual atmospheric effects in the reflectance spectra measured, which

varied depending upon the thickness of atmosphere beneath the platform. The systematic nature of these variations suggested that an airframe-mounted irradiance sensor would be a useful addition to an aircraft sensor for atmospheric correction purposes, allowing the calculation of at-sensor reflectance and the temporal and spatial variability of the incident irradiance (Gray *et al.*, 1997). However, the apparent usefulness of a rooftop probe is seriously compromised in data acquisition from fixed-wing platforms due to variations in downwelling irradiance signals caused by pitch, roll, and yaw of the platform.

Shepherd *et al* (1995) have analysed the errors involved in using data from a rooftop-mounted incident irradiance sensor fitted to the Itres Instruments Compact Airborne Spectrographic Imager (CASI) to calculate the reflectance of ground targets. Piekutowski *et al.* (1996) attempted to correct for variation in aircraft attitude on data from an incident light sensor fitted to the MEIS-II (Multispectral Electro-optical Imaging Scanner) (Piekutowski, *et al.*, 1996). However, their attitude correction still needs the 5S radiative transfer model to estimate the ratio of direct to diffuse irradiance at altitude.

## 2. Slope Irradiance Model

In practice, the aircraft attitude is always tilting toward a certain direction during the flight. As a cosine diffuser is mounted parallel to the body of the plane, the slope of the probe corresponds to the aircraft attitude. The irradiance on the cosine diffuser inclined toward the sun is greater than that on the horizontal plane, and vice versa.

There have been a number of empirical and analytical studies of irradiance on slopes (e.g. Brunger and Hooper, 1993; Gates, 1980), often developed for estimating the efficiency of solar panels to be used inclined on the top of buildings (Hooper and Brunger, 1980). The diffuse irradiance on the inclined surface is obtained by integrating the sky radiance distribution model over the sky dome visible to the surface with the horizontal global and diffuse irradiance measurements.

The simplest slope irradiance model basically assumes that the diffuse sky radiation is uniformly distributed over the dome. In this isotropic model the total irradiance is only a function of slope angle,

$$G_{d,i} = G_d (1 + \cos(\alpha))/2 \quad (1)$$

The isotropic model normally underestimates the diffuse irradiance from clear sky conditions and approximates prediction of completely overcast conditions. At the other extreme, the diffuse irradiance may be modelled as a heliocentric function in which the total irradiance is a function of the angular distance from the sun to a point in the sky,

$$G_{d,i} = G_d (\cos(\alpha) + \sin(\alpha) \cos(\phi) \tan(\theta)) \quad (2)$$

The heliocentric model greatly overestimates the diffuse radiation as the slope inclines toward the sun. These two models represent the extreme sky conditions and are rather unrealistic. Many authors have developed models to predict various sky conditions, including Hooper and Brunger (1980, 1987) (radiance model) and Perez (1993a, b) (luminance model). The performance of these different model were compared by Vartiainen (2000), and Perez's model (Perez, 1993a & 1993b) turned out to have the lowest error range amongst five sky irradiance and six sky radiance distribution models on slope. Brunger and Hooper's model (1993) is used in this study as it is one of the few sky radiance distribution models that cover the complete range of atmospheric conditions.

Although there is evidence indicating that radiance (unit  $W/m^2sr$ ) and luminance (unit  $lumen/m^2sr$ ) distributions are qualitatively similar, the radiance distribution model is more sensible for RS applications. Another important feature of the model is that it is a function of two parameterised atmospheric conditions, the atmospheric clarity index ( $k_t$ ) and diffuse fraction ( $k$ ).

The model used in this study is based on the Three-Component Continuous Distribution (TCCD) model of [Hooper and Brunger \(1980\)](#) which comprises circumsolar ( $a_0$ ), horizontal brightening ( $a_1$ ), and uniform background terms ( $a_2$ ). An extra coefficient ( $a_3$ ) is set as a linear term. The model calibration was undertaken by finding the parameters. A number of field experiments under a wide variety of atmospheric condition were sorted into bins defined by specific ranges of  $k_t$  and  $k$ . The set of measurements in each bin were statistically analysed for the model parameters.

Once the atmospheric condition had been selected, its corresponding parameters were used to calculate the radiance ( $W/m^2sr$ ) of the sky over the whole hemisphere ( $\theta, \phi$ ),

$$L(\theta, \phi, \theta_s, \phi_s) = G_d \left[ \frac{a_0 + a_1 \cos \theta + a_2 \exp(-a_3 \Psi(\theta, \phi, \theta_s, \phi_s))}{\pi(a_0 + 2a_1/3) + 2a_2 I(\theta_s, a_3)} \right]^1 \quad (3)$$

The distribution of radiance over the hemisphere on a slope is used to calculate the ratio of sky irradiance on the slope to that which would have been found on a horizontal surface, and to integrate the radiance over the sky dome visible to the surface.

$$G_{d,i} = G_d \frac{\int_{-\pi}^{\pi} \int_{\alpha_0}^{\pi/2} L(\theta, \phi, \theta_s, \phi_s) \cos \theta (\sin \theta \cos \alpha + \cos \theta \sin \alpha \cos \phi) \cdot d\phi d\theta}{\int_{-\pi}^{\pi} \int_0^{\pi/2} L(\theta, \phi, \theta_s, \phi_s) \cos \theta \sin \theta \cdot d\phi d\theta} \quad (4)$$

Depending on whether the position of the point on the dome is below horizon or not, the limit of inner integration is given by,

$$\alpha_0 = \begin{cases} 0 & \text{Where } -\pi/2 \leq \phi \leq \pi/2 \\ \arctan(-\tan \alpha \cos \phi) & \text{Otherwise} \end{cases} \quad 0$$

---

<sup>1</sup> Where

$$I(\theta_s, a_3) = \frac{[1 + \exp(-a_3 \pi/2)]}{(a_3^2 + 4)} \cdot \left\{ \pi - \left[ 1 - \frac{2[1 - \exp(-a_3 \pi)]}{\pi a_3 [1 + \exp(-a_3 \pi/2)]} \right] \cdot [2\theta_s \sin \theta_s - 0.02\pi \sin(2\theta_s)] \right\} \quad (5)$$

and the angular distance in radians between  $(\theta, \phi)$  and  $(\theta_s, \phi_s)$ ,

$$\Psi(\theta, \phi, \theta_s, \phi_s) = \arccos[\sin \theta \sin \theta_s \cos(\phi - \phi_s) + \cos \theta \cos \theta_s] \quad (6)$$

### 3. Data Description

On 3 September 1999 the intertidal vegetation bordering the West Solent, Hampshire, UK, was surveyed using CASI from the Environment Agency (EA) on behalf of English Nature. Over 30 flightlines were flown at an altitude of 2,500 feet between 09:00 and 12:40. The CASI was configured in spatial mode using the intertidal bandset recommended by [Thomson \*et al.\* \(1998\)](#).

Table 1. Flight information overpass of the calibration site. Figures in brackets indicate information in \*.inf file, which are suspected as being in error, based on the map provided and the image orientation.

Image	Time (GMT)	Heading (Degree from the North)	Solar Azimuth (Degree from the North)	Relative sun angle (= heading–solar azimuth)
Imag4315	9:20:16 to 9:21:35	232	126	106
Imag4332	10:40:16 to 10:41:56	55	150	-95
Imag4349	12:13:36 to 12:15:44	175 (151)	184	-9
Imag4350	12:18:56 to 12:21:04	341 (331)	185	156
Imag4354	12:36:20 to 12:37:37	231 (331)	191	40

During the period of the aerial survey, three flight lines (Imag4315, Imag4332, and Imag4354) passed over the Beaulieu Heath Calibration Site (BHCS; approximately  $N50^{\circ} 50'$ ,  $W1^{\circ} 25'$ ) where a Spectron SE-590 spectroradiometer was located and continuously measuring downwelling irradiance over the spectral range from 368 to 1114 nm. The data from the SE-590 were integrated over the spectral range and plotted for the series of measurements ([Figure 1](#)). The solar flux reaching the ground is modelled by using the 6S code and superimposed upon the ground measurements. The difference between them (grey region in [Figure 1](#)) increased slightly with time. Between around 09:00 and 10:45 the solar irradiance steadily increased as the early morning mist cleared, and there was an interval during which the solar irradiance changed rapidly as high level cloud passed over the area. Soon after such disturbances, the irradiance became stable, and remained so until the end of the survey.

The flightlines of Imag4349 and Imag4350 were selected in order to test whether the method could compensate for the effect of different flight direction upon data from the ILS. These flightlines represent almost the worst case possible, with Imag4349 being flown almost directly into the Sun (relative solar azimuth  $-9^{\circ}$ ) and Imag4350 being flown almost directly away from the Sun (relative solar azimuth  $156^{\circ}$ ). The area covered by flightlines Imag4349 and Imag4350 was approximately 9km north of the site at which solar irradiance was measured at the ground, and it is assumed that similar conditions prevailed at both sites. Figure 1 shows that the solar irradiance during the period of these flightlines was almost constant.

In the CASI system, the incident light sensor (ILS) is a cosine-corrected receptor fitted horizontally in the roof of the aircraft ([Figure 2](#)). The sensor head is connected to the CASI via an optical fibre. Light from the ILS is imaged onto the hidden section of a two-dimensional CCD array, and recorded in spectral bands identical to those from the scene viewed by the CASI. As the CASI was configured in spatial mode, the ILS data are recorded in column of 512 in each line of image data. No calibration of ILS data to irradiance units was available for this particular sensor. The data from the ILS are strongly affected by the direction of flight relative to the sun,

i.e. a mean ILS of Imag4332, a flightline away from the sun, is lower than irradiance at ground whereas the others are greater as the flightline is heading relatively toward the sun.

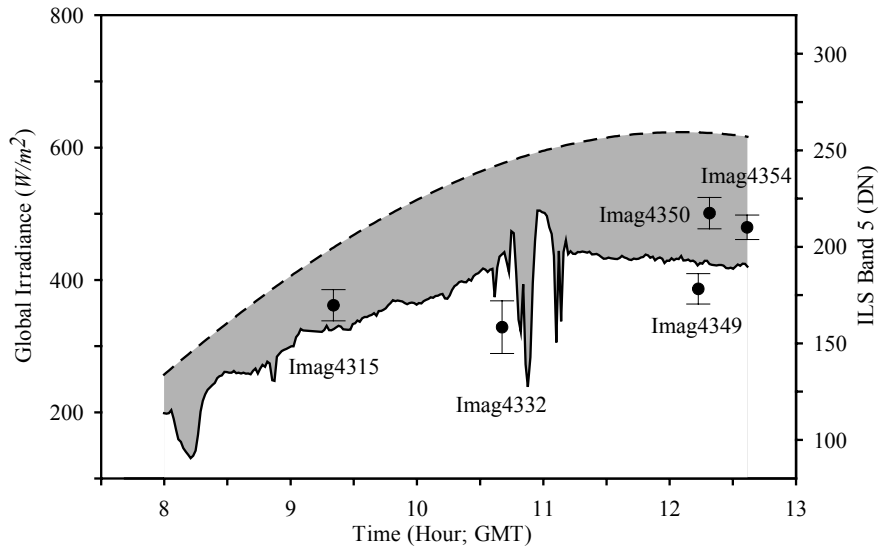


Figure 1. Global irradiance at ground in Beaulieu Heath calibration site (solid line), and the solar flux modelled by 6S (dashed line). The grey area between dashed and solid lines represents the difference between those two. The mean DN values of the ILS from three flights over the calibration site are superimposed with their standard deviation ranges, as are the mean DN values from the two test flightlines (Imag4349 and Imag4350)

Since a cosine receptor mounted on an aircraft is sensitive to the inclination of the sensor in relation to the sun, it is necessary to take account the deviation of the aircraft from level flight. Attitude parameters of pitch and roll were recorded in DN for every line of the image, and converted to angles in degrees by post-processing. A positive pitch indicated the nose of the aircraft rising above the horizon, and vice versa. A positive roll represented the port wing dropping below the horizon. Yaw was not recorded for the particular CASI installation we used. Plots of pitch and roll recorded during the flights show that pitch is positive at around  $20^\circ$  depending on the speed of the plane, while roll values fluctuate throughout the flightline.



Figure 2. CASI Incident Light Sensor (ILS) (Source: <http://www.itres.com/>).

#### 4. Results

Brugger and Hooper's model (1993) described above was applied to the ILS data. The model was originally developed in order to calculate the irradiance on a slope ( $G_{d,i}$ ) from known atmospheric conditions ( $k_t$ ,  $k$ ). In the case of the ILS data, on the other hand, the objective is to use the measurements made by the inclined sensor to calculate the irradiance in the horizontal plane at sensor altitude, as well as to determine the atmospheric conditions.

To achieve this result it is necessary to invert the model, although it is not a true inverse (Figure 3). A table of the model coefficients obtained by intensive field experiments over a wide variety of atmospheric conditions was used as input data. A total of 48 sets of model coefficients over specific ranges of  $k_t$  and  $k$  were applied to the model with solar positions ( $\theta_s$ ,  $\phi_s$ ), slope angle ( $\alpha$ ), and direction relative to the sun.

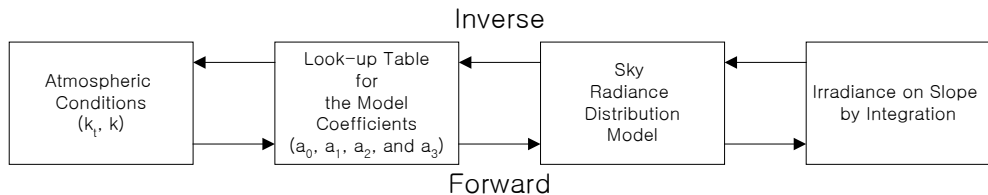


Figure 3. Schematic diagram of sequence of Brunger and Hooper's model.

The aircraft attitude data had to be pre-processed before applying the model. To find the accurate degree of slope and its direction is significant as the model is sensitive to the inclined surface in relation to the sun position. The aircraft attitude is expressed by pitch and roll with respect to the flight direction. Although pitch is greater than roll (see [Figure 5a](#)) so that flight direction may be considered as fixed slope direction during the flight, line-by-line calculations using pitch and roll result variations of more than  $\pm 10^\circ$  in slope direction and  $\pm 5^\circ$  in slope angle. Such variations in slope causes equivalent differences in sun position.

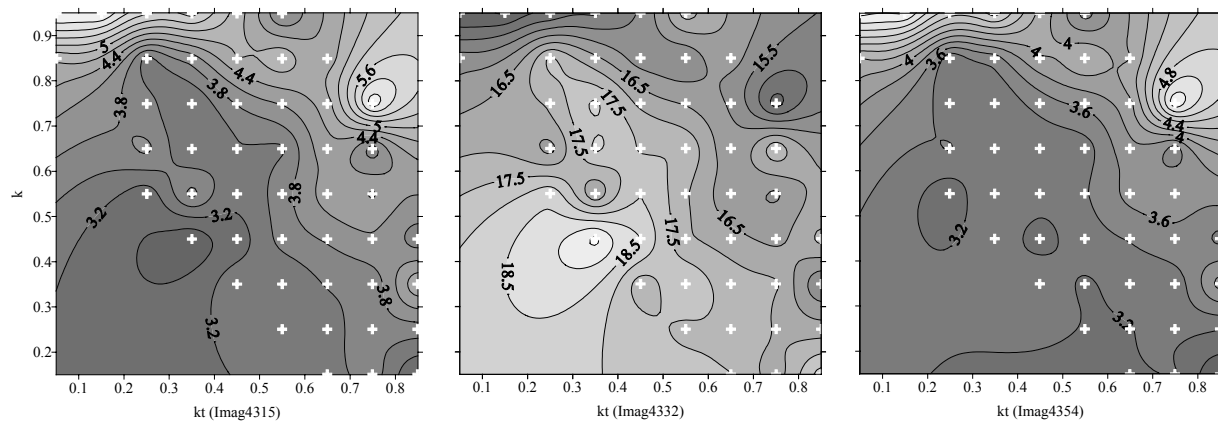


Figure 4. RMS contour plots over the look-up table of atmospheric condition ( $k_t, k$ ). White crosses represent the points of available model coefficients (Brunger and Hooper, 1993).

#### 4.1 ILS data over calibration site

Since each flightline took less than 2 minutes over a linear distance of less than 10 km, it was assumed that atmospheric condition above at-sensor level were relatively uniform and constant. Therefore, the irradiance on the horizontal surface calculated from the model was assumed to be constant as well. The uniformity of the irradiance over line number of each image data was found using the Root Mean Square (RMS) deviation as a convenient measure of the spread around the mean. The lowest region in the look-up table represented the most appropriate value for the ILS correction. The contour plots of RMS in each flightline show that the position of the lowest RMS region varied, indicating atmospheric conditions changed during the survey (Figure 4). In comparison with the field measurements during the flights (Figure 1), Imag4315 was affected by the early morning mist and results show relatively low atmospheric clarity index ( $k_t = 0.35$ ) with moderate diffuse ratio ( $k = 0.45$ ). Imag4332 was collected just before the high level cloud ( $k = 0.75$ ), while steady increases of irradiance was about to settle ( $k_t = 0.75$ ). In the last flight (Imag4354), atmospheric conditions above the altitude of the flight became clear and stable. The atmospheric clarity index ( $k_t = 0.85$ ) was similar to the previous flight (Imag4332).

and the amount of irradiance at the ground in both flights was similar, though it was more unstable in Imag4332, but the proportion of diffuse irradiance with respect to the global irradiance was reduced ( $k = 0.15$ ).

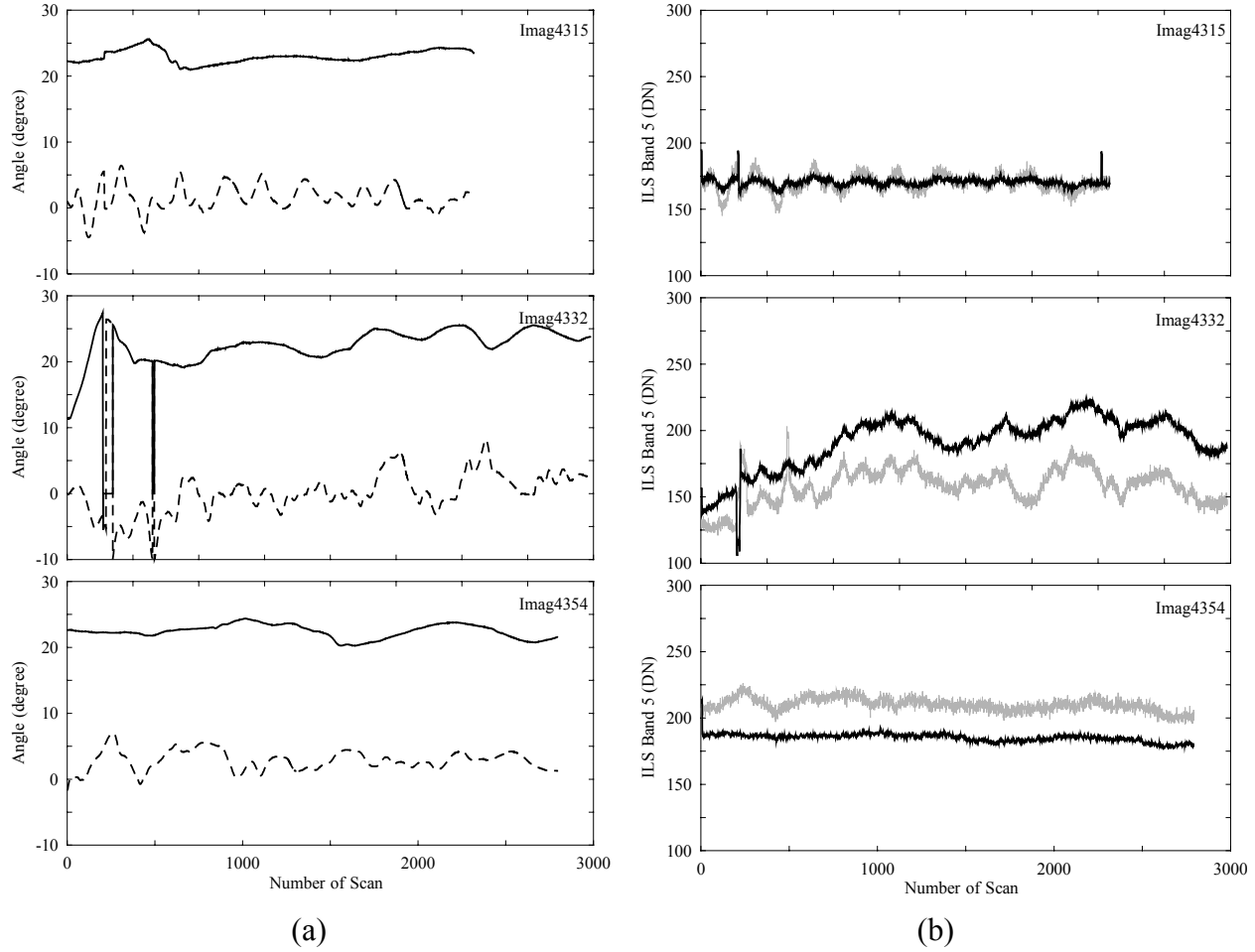


Figure 5. Plots of pitch (solid line) and roll (dotted line) in each flight (a). In (b), 7-scan-averaged raw ILS (grey) is superimposed on the model corrected ILS plots (black).

The model coefficients determined in each flight from the parameterised atmospheric conditions above were used for the irradiance on a horizontal surface at sensor level (Figure 5b). In order to reduce the high frequency errors and outliers, the ILS data were averaged over 7 scans. The effects of aircraft attitude on the ILS data are effectively minimised, and the corrected ILS values decrease in Imag4315 and Imag4354 while they increase in Imag4332. The mean values after correction follow the trend of irradiance changes at ground quite well (see Figure 1). The variations, still shown after the correction, may be due to errors in the ILS calibration or to actual atmospheric variations over the area. The ILS correction on Imag4332 is rather poorer than the others and may be due to unstable atmospheric conditions during this flightline, or possibly incorrect information on flight direction (E.M. Rollin, personal communication).

In addition to atmospheric characteristics and ILS correction from aircraft attitude, at-sensor sky radiance distributions were given by the model calculations (Figure 6). The radiance of the sky was calculated by using Equation 3. Stereonet plots of the sky distribution during the acquisition of Imag4315 and Image4354 show a similar pattern whereas that from Imag4332 looks close to the radiance distribution under a cloudy sky. On the other hand, the magnitudes of the radiance are similar in Imag4332 and Imag4354, both being much larger than Imag4315 which has radiance more concentrated in the sun's direction.

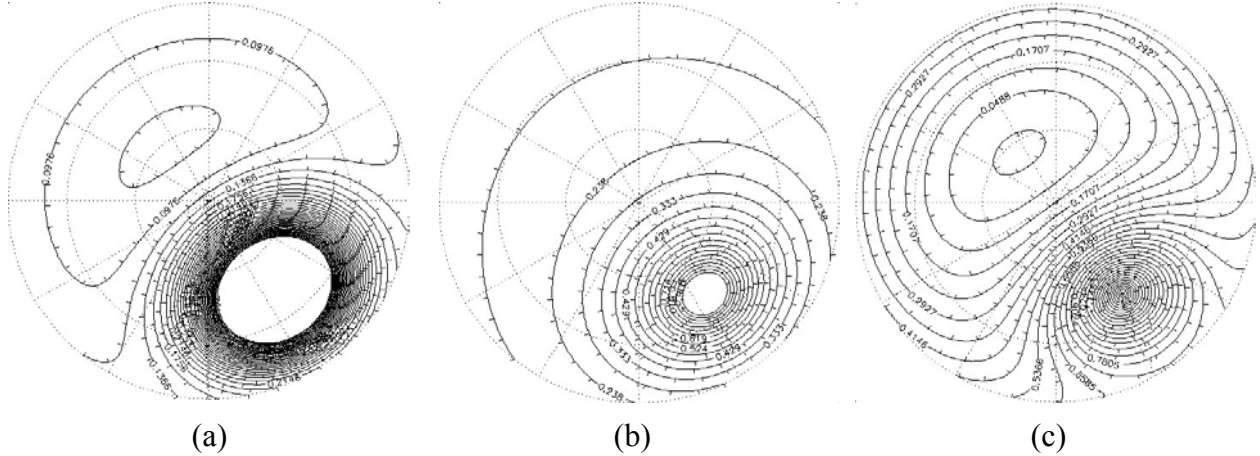


Figure 6. Stereonet representation of the sky radiance distribution for each of the three flights: Imag4315 (a), Imag4332 (b), and Imag4354 (c), and calculated using the Brunger and Hooper model.

## 4.2 Comparing ILS data in different flight directions

Since the variation of pitch is mainly responsible for the orientation of the detector, the average flight direction shows how the sun position changes relative to the slope of the receptor. Amongst more than 30 flightlines during the project, two images were selected for testing the model. Imag4349 was flown into the sun, whereas Imag4350 was in opposite direction. The ILS data were greatly increased when the plane away toward the sun, due to the receptor being tilted towards the primary source of illumination, and vice versa.

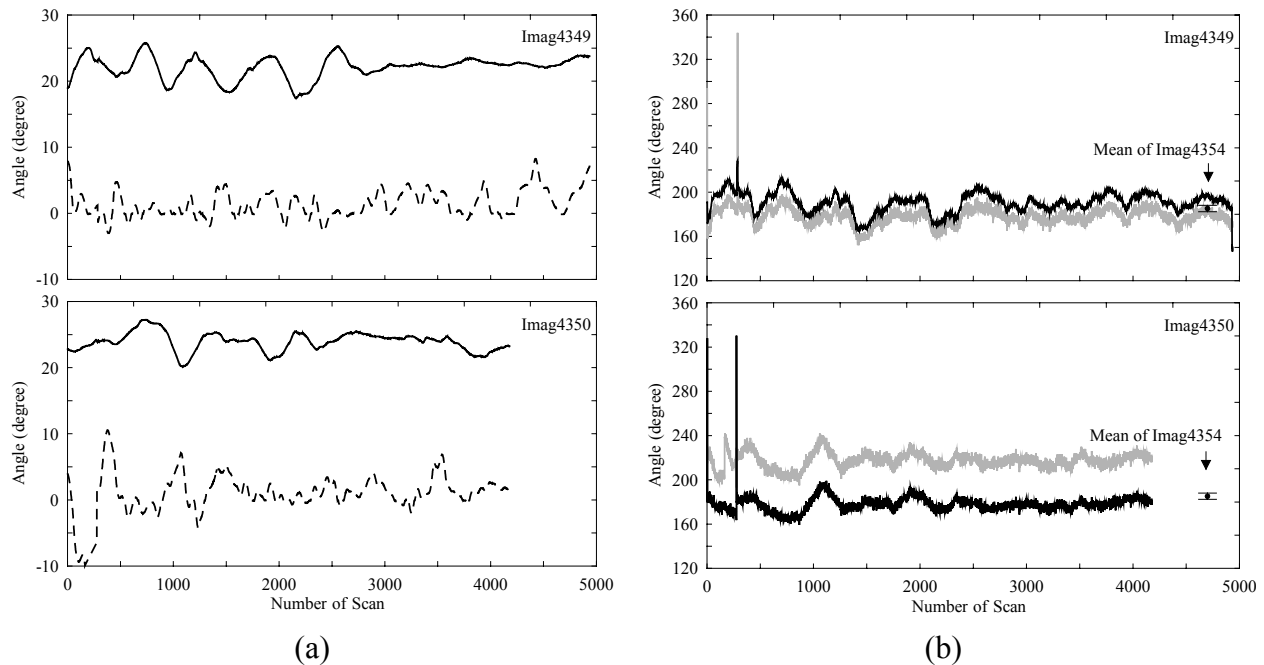


Figure 7. Plots of pitch (solid line) and roll (dotted line) in each flight (a). In (b), 7-scan-averaged raw ILS (grey) is superimposed on the model corrected ILS plots (black). The error bars in plot (b) represent the range of standard deviation of model calculation in Imag4354.

Figure 7a shows plots of aircraft attitude during the acquisition of Imag4349 and Imag4350. Like the others, pitch angles are generally larger than roll, and their means are greater than 20°. The comparison of the plane attitudes with the ILS show that changes of the ILS data corresponds to changes in the orientation of the plane. The ILS data was again applied to the

model and a correction derived. Figure 7b shows the results of applying the correction method to data from flightlines Imag4349 and Imag 4350. As would be expected from the flight directions, ILS data from Imag4349 have increased, while those from Imag4350 have decreased. The results show some reduction in the effect of aircraft attitude, but not a complete correction. However, the model has succeeded in correcting the mean spectral irradiance from the two flightlines, which is much closer than in the raw data, and is more representative of that measured on the ground at the calibration site (Figure 8). The failure of the model to correct for all the effects of aircraft attitude may be because the yaw direction was not recorded precisely (unlike pitch and roll). A small error in yaw would have a relatively large effect upon the ILS value at these extreme conditions of relative solar azimuth.

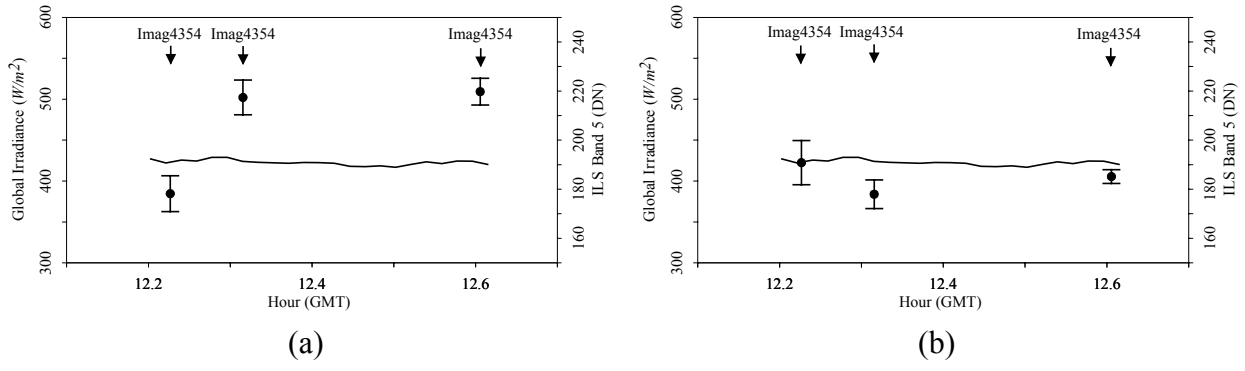


Figure 8. Comparison between mean DN values of ILS data from the two test flightlines (a) before correction and (b) after correction. The error bars indicate one standard deviation either side of the mean. Also there is a plot of the mean DN values of ILS data from flightline Imag4354 that passed over the calibration site shortly after the two test flightlines. The solid line in each plot represent irradiance measurements at ground level during the flight. Scales between global irradiance and ILS DN are the same as shown in Figure 1.

## 5. Conclusion

A sky radiance distribution model developed by Brunger and Hooper (1993) has been applied to CASI Incident Light Sensor data in order to estimate the downwelling solar irradiance at the aircraft. Continuous slope changes of the ILS sensor due to variations of the aircraft attitude is a problem in the direct use of the ILS data, but this helps in finding optimum coefficients for the model. The model results in a unique set of coefficients for each flightline, which relate to the parameterised atmospheric condition. The method was used to correct ILS data from three flightlines flown at relative solar azimuths from  $-9^\circ$  to  $+156^\circ$ . Use of the model increased the accuracy of the mean DN value retrieved from the ILS, however, some attitude-induced variations remained in the ILS data. This means that the method will require further work before it can be used as a line-by-line correction for the effect of the atmosphere. This remains the long-term goal, but the results presented here show that the method can also provide an average flightline-specific correction for ILS data collected under stable illumination, and can also provide an estimate of the irradiance distribution at sensor level, both of which are key to accurate and timely atmospheric correction of airborne sensor data.

## 6. Glossary

$a_0, a_1, a_2, a_3$	Parameters of assignable value that allow the sky radiance model to respond to the atmospheric radiation conditions
$G_d$	Diffuse irradiance on a horizontal plane
$G_{d,I}$	Diffuse irradiance on an inclined surface

$G_h$	Global solar irradiance on a horizontal surface
$K$	Diffuse fraction, $G_d/G_h$ . A ratio of the diffuse irradiance on a horizontal surface to the global irradiance on a horizontal surface. Ranges from 0 to 1
$k_t$	Atmospheric clarity index. $G_h$ divided by the local extraterrestrial solar irradiance on a horizontal surface; the extraterrestrial solar irradiance is a deterministic function of date, time, and the local latitude. Ranges from 0 to 1.
$L$	Sky radiance
$\theta$	Angular distance from the zenith in radians
$\phi$	Azimuth angle measured in radians clockwise in the horizontal plane from the North
$(\theta_s, \phi_s)$	Coordinate of the direction of the sun
$\Psi$	Angular distance in radians between the direction of the solar disk and the direction $(\theta, \phi)$
$\alpha$	Slope of the aircraft

## 7. Acknowledgements

The authors gratefully acknowledged the provision of CASI and aircraft attitude data from the UK Environmental Agency. Jennifer Youngberg, University of Waterloo, Canada, kindly provided an original source code of the model. Kyu-Young Choi is grateful for funding from the University of Southampton High Performance Computing Initiative. The UK Natural Environment Research Council Equipment Pool for Field Spectroscopy supported this work through advice from Dr Elizabeth Rollin and by the loan of a field spectroradiometer.

## 8. References

Brunger, A. P., Hooper, F. C., 1993, Anisotropic sky radiance model based on narrow field of view measurements of shortwave radiance, *Solar Energy*, **51**, 1, 53-64, Erratum: **51**, 6, 523p.

Gates, D.M., 1980, *Biophysical Ecology*, Springer-Verlag, New York, 611p.

Gray, L., Freemantle, J., Shepherd, P., Miller, J., Harron, J., Hersom, C., 1997, Characterization and Calibration of the CASI airborne imaging spectrometer for BOREAS, *Canadian Journal of Remote Sensing*, **23**, 2, 188-195p.

Hooper, F. C., Brunger, A. P., 1980, A model for the angular distribution of sky radiance, *Journal of Solar Energy Engineering*, **102**, 196-202p.

Hooper, F. C., Brunger, A. P., Chan, C. S., 1987, A clear sky model of diffuse sky radiance, *Journal of Solar Energy Engineering*, **109**, 9-14p.

Milton, E.J., Blackburn, G.A., Rolling, E.M., Danson, F.M., 1994, Measurement of the spectral directional reflectance of forest canopies: a review of methods, and a practical application, *Remote Sensing Review*, **10**, 285-308.

Perez, R., Seals, R., Michalsky, J., 1993a, All-weather model for sky luminance distribution – Preliminary configuration and validation, *Solar Energy*, **50**, 235-245.

Perez, R., Seals, R., Michalsky, J., 1993b, Erratum to All-weather model for sky luminance distribution – Preliminary configuration and validation, *Solar Energy*, **51**, 423.

Piekutowski, T., O'Neil, N., Leckie, D., Beaubien, J., Shepherd, P., 1996, Radiometric correction of MEIS-II imagery using airborne irradiation measurements, In *Proceedings of 26<sup>th</sup> International Symposium on Remote Sensing of Environment and 18<sup>th</sup> Annual Symposium*

*of the Canadian Remote Sensing Society*, Vancouver, British Columbia, Canada, 458-462.

Shepherd, P.R., O'Neil, N.T., Piekutowski, T., 1995, Analysis of downwelling and upwelling diffuser probe data to determine at-sensor irradiance fluxes, In *Proceedings of the 17<sup>th</sup> Canadian Symposium on Remote Sensing*, Canadian Remote Sensing Society, Saskatoon, Saskatchewan, June 13-15, 337-342.

Shepherd, P.R., Xu, Q. F., 1993, An error analysis of a reflectance conversion methodology using an irradiance sensor, In *Proceedings of 16<sup>th</sup> Canadian Symposium on Remote Sensing*, 841-845p.

Song, C., Woodcock, C.E., Seto, K.C., Lenney, M.P., Macomber, S.A., 2001, Classification and change detection using Landsat TM data: When and how to correct atmospheric effects?, *Remote Sensing of Environment*, **75**, 230-244.

Stokkom, H.T.C. van, Guzzi, R., 1984, Atmospheric spectral attenuation of airborne remote-sensing data comparison between experimental and theoretical approach, *International Journal of Remote Sensing*, **5**, 925-938.

Thomson, A.G., Fuller, R.M., Sparks, T.H., Yates, M.G., Eastwood, J.A., 1998, Ground and airborne radiometry over intertidal surfaces: Waveband selection for cover classification, *International Journal of Remote Sensing*, **19**, 1189-1205.

Vartiainen, E., 2000, A new approach to estimating the diffuse irradiance on inclined surface, *Renewable Energy*, **20**, 45-64p.

Wilson, A.K., 1995, *NERC Scientific Services Airborne Remote Sensing Facility User Guide*, Natural Environment Research Council, 72p.